Applied Ocean Research 123 (2022) 103154

Contents lists available at ScienceDirect

Applied Ocean Research

journal homepage: www.elsevier.com/locate/apor

# Suppression of vortex-induced vibration of a rigid cylinder using flexible shrouding

Nur Ain Shafiza Ramzi [a], Lee Kee Quen [a,*], Hidetaka Senga [b], Hooi-Siang Kang [c,d], Meng Hee Lim [e], Noor Idora Mohd Sukarnoor [a]

[a] Intelligent Dynamic and System I-kohza, Malaysia-Japan International Institute of Technology, Universiti Teknologi Malaysia, Kuala Lumpur, Malaysia
[b] Department of Naval Architecture and Ocean Engineering, Graduate School of Engineering, Osaka University, Japan
[c] School of Mechanical Engineering, Faculty of Engineering, Universiti Teknologi Malaysia, Malaysia
[d] Marine Technology Center, Institute for Vehicle System and Engineering, Universiti Teknologi Malaysia, Malaysia
[e] Institute of Noise and Vibration, Universiti Teknologi Malaysia, Kuala Lumpur, Malaysia

ARTICLE INFO

*Keywords:*
Vortex-induced vibration
Rigid cylinder
Suppression
Flexible shrouding

ABSTRACT

Experimental investigations were conducted to address the reduction of vortex-induced vibration (VIV) and mean drag coefficient ($C_{d\ mean}$) acting on the oscillating cylinder fitted with a shroud of various parameters. The effectiveness of the shrouds in suppressing the VIV of a short rigid cylinder was investigated by varying the mesh size (B) and mesh thickness (H). The experiments were performed in water flume in NAHRIM and data analysis of Cross-Flow (CF) and In-Line (IL) vibration amplitudes, IL and CF frequencies, mean drag coefficient responses were carried out. Calculation of the laminar boundary layer thickness around a circular cylinder was carried out as a benchmark in deciding the thickness of the mesh. The effect of mesh size and mesh thickness of shrouds was also addressed in this article. From the results obtained, it can be observed that the shroud with mesh size $B = 0.2D$ and mesh thickness $H = 0.03D$ achieved an optimum condition where it was able to suppress the amplitude without increasing $C_{d\ mean}$, with 76.62% of amplitude reduction and 48.40% of $C_{d\ mean}$ reduction.

## 1. Introduction

The study of vortex-induced vibration (VIV) on the short cylinders has drawn interest of a large number of researchers. However, the majority of the studies regarding shroud focused on cylinders with one degree of freedom (1dof) i.e. the cylinders vibrate only in the transverse direction of the incident flow (Kumar et al., 2018; M.M. Cicolin and Assi, 2017; M.M. Cicolin and Assi, 2017; Huera-Huarte, 2017). Due to the offshore demand, cylinders with two degree of freedom (2dof) became the subject of research and researchers have recently focused on riser systems that are connected to offshore platforms. Additionally, experiments with low mass ratios are needed in order to simulate the idealized conditions encountered in real-world ocean applications (M.M. Cicolin and Assi, 2017).

Vortex shedding behind bluff bodies is a natural effect when flow around the structure is disturbed by the shape of the bluff bodies. The vortex is generated when fluid flows past the pipe structure. This is because of the presence of shear in the boundary layer (Ranjith et al., 2016). The strength of each shear layer increases away from the pipe, and it continues to grow until a stronger opposing shear layer breaks off the former shear layer, resulting in vortex shedding of the downstream of pipe (Bearman, 1984). The vortex shedding causes fluctuating forces, namely the lift and drag forces that induce the cross-flow (CF) and in-line (IL) vibrations, respectively (Zhou et al., 2011). The continuous high oscillating vibration amplitude can lead to great fatigue damage and reduce the fatigue life of the cylinder (Gao et al., 2015). VIV is a prominent element in creating fatigue damage as the riser system is exposed to unexpected marine environments such as waves and currents (Kim et al., 2018), (Liu et al., 2020). This will directly lead to fracture of pipe and the possibility of oil leakage and oil rig explosion. Mumbai High North disaster in the Indian Ocean is one of the world's worst offshore oil rig disasters due to riser rupture (Praveen Duddu, 2021).

In order to reduce the VIV, researchers have proposed many ideas to overcome this problem such as fairings, strakes, ventilated trousers, etc. The proposed methods have been investigated experimentally or numerically in the past decade. Helical strakes showed good performance in amplitude reduction but at the same time generated drag force that is unwanted (Ranjith et al., 2016). The advantage of fairing is that it

* corresponding author
*E-mail addresses:* nashafiza2@graduate.utm.my (N.A.S. Ramzi), lkquen@utm.my (L.K. Quen).

https://doi.org/10.1016/j.apor.2022.103154
Received 26 October 2021; Received in revised form 7 March 2022; Accepted 22 March 2022
Available online 9 April 2022

**Table 1**
Properties of cylinder.

| | |
|---|---|
| Outer diameter ($D$) | 0.033 m |
| Inner diameter ($d$) | 0.002 m |
| Total length ($L$) | 0.340 m |
| Total spring stiffness ($k_T$) | 115.118 N/m |
| Plate diameter ($D_P$) | 0.130 m |
| Plate thickness ($T_P$) | 0.005 m |
| The total mass of pipe including plate (m) | 0.300 kg |
| Aspect ratio ($L/D$) | 10.300 |
| Mass ratio ($m^* = 4m/\pi D^2 L_p$) | 1.031 |
| Reduced velocity ($U_r = U/f_n$D) | 1.720 −8.800 |
| Damping ratio ($\zeta = 1/2\pi \ln y_n/y_{n+1}$) | 0.0116 |
| Reynolds number ($R_e = \rho UD/\mu$) | 3708 - 18,910 |

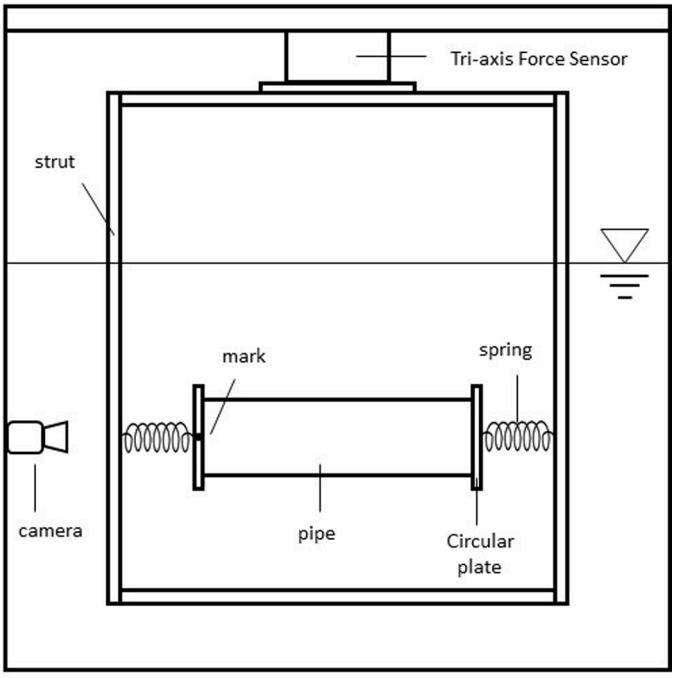


**Fig. 1.** Schematic view of the experimental set-up in the water flume.

**Table 2**
Matrix of shroud combinations implemented for study.

| **Mesh size** | **B1 = 0.2*D*** | **B2 = 0.4*D*** | **B3 = 0.6*D*** | **B4 = 0.8*D*** |
|---|---|---|---|---|
| H1 = 0.03*D* | 0.2D 0.03*D* | 0.4D 0.03*D* | 0.6D 0.03*D* | 0.8*D* 0.03*D* |
| **Mesh thickness** | **H1 = 0.03*D*** | **H2 = 0.09*D*** | **H3 = 0.11*D*** | |
| B3 = 0.6*D* | 0.6D 0.03*D* | 0.6D 0.09*D* | 0.6D 0.11*D* | |

retains the ability to rotate. Otherwise, de-stabilizing forces can be created. However, the fairing can be costly and time-consuming to be installed (Allen et al., 2007; Zhu et al., 2017). Jiménez-gonzález and Huera-Huarte (Jiménez-gonzález and Huera-huarte, 2018) have located a pair of control rods with varying sizes around the cylinder and found several mechanisms that cause large modifications within the wake which also affects the VIV responses. As the perturbation in the cylinder's wake was positioned near the cylinder's surface, it induced major changes in the boundary layer development over the cylinder. There was a particularly sensitive area where the shear layers interact if the perturbation was located further away from the surface. Meanwhile, Zhu and Yao (Zhu and Yao, 2015) and Silva-Ortega and Assi (Silva-Ortega and Assi, 2017) disrupted the shear layer interaction region using control rods. To take advantage of the same phenomena as the control rod, Huera-Huarte (Huera-Huarte, 2017) proposed the application of meshes in order to suppress VIV. The advantage of meshes is that it is omnidirectional, which is independent of the flow of direction. On the other hand, a combination of net substructure, called Ventilated Net (VN) or shroud, has attracted the attention of researchers recently. Cicolin and Assi (M.M. Cicolin and Assi, 2017) investigated the Ventilated Trousers (VT), a shroud composed of a flexible net fitted with three-dimensional bobbins. The VT is able to suppress the peak amplitude of vibration by 40%. Brown and King (Brown et al., 2008) also used VT to reduce riser drag, suppress VIV and limit drilling downtime. Besides, King et al. (King et al., 2013) found a reduction of about 90% of VIV amplitudes for riser with VT at post-critical $Re$ ($1.2 \times 10^6$). Although same studies have been conducted, the investigation on the shroud is not widely explored by researchers. To explore the possibility of improvement, the mesh size of the shroud and the thickness of the mesh were taken into consideration. Based on the previous studies, some contradictions are reported in the mesh size, where the increase in the mesh size of the shroud around the pipe showed better performance in attenuating VIV (Kumar et al., 2018). On the other hand, Huera-Huarte (Huera-Huarte, 2017) obtained an opposing result, where a small mesh size seemed to perform better in his study. These conflicts gained our interest to look into this matter further in detail. The main purpose of the present study is to investigate the effectiveness of the shroud in reducing VIV and mean drag coefficient ($C_{d\ mean}$).

## 2. Methodology

### 2.1. Experimental set-up

The experiments were carried out in NAHRIM water flume. The dimension of the water flume was 50 m long, 0.75 m wide and 0.70 m deep. The flow generated by the water flume pump was controlled by a speed inverter system that is able to generate uniform flow varied from 0.1 m/s to 0.51 m/s with an interval of 0.03 m/s, yielding Reynolds number from 3708 to 18,910. The circular cylinder model consisted of a bare-hollow Polyvinyl Chloride (PVC) pipe with length $L = 0.34$ m and diameter $D = 0.033$ m. The inside of the model was filled with water as it was fully submerged in the water flume. The other properties of the cylinder are tabulated in Table 1. The model had a transparent end-plate attached to its left and right end in order to hold the shroud. Two springs were connected to the model to allow motions in the IL direction and the CF direction of the flow. The experimental design followed a previous study (Senga et al., 2018). The schematic diagram of the experimental setup is shown in Fig. 1.

### 2.2. Shrouds

Cicolin et al. (Cicolin et al., 2014) found that the shroud's mesh can reduce VIV by affecting the shear layers and preventing them from interacting with each other, thereby subduing vortex shedding. In designing the shroud, the parameters to be considered are the mesh size (B) and mesh thickness (H) as shown in Table 2.

The shroud radius ($r$) was set to be constant at $1.3D$ after reviewing the previous studies in both rigid and flexible cases. For the rigid case, most of the studies focus on large radius of shrouding ($r$). Huera-Huarte (Huera-Huarte, 2017) showed the best performance in suppressing VIV with $r = 1.3D$. Besides, M. M. Zdravkovich & J. R. Volk (Zdravkovich and Volk~, 1972) stated that $r = 1.25D$ was the optimum ratio of shrouding radius in their study.

On the other hand, for the flexible case, few studies (Kumar et al., 2018)–[3] referred the suggestion of Brown et al. (King et al., 2013), where the proposed shrouding radius was $r = 0.75$D. Meanwhile, Kumar et al. (Kumar et al., 2018) varied their shrouding radius by including two additional values ($r = 0.875D$ and $1D$). Unexpectedly, the shroud with the largest radius ($r = 1D$) was able to suppress VIV and drag force very well in their study compared to the previous researches (M.M. Cicolin and Assi, 2017)–[3], (Cicolin et al., 2014). By referring to the rigid and

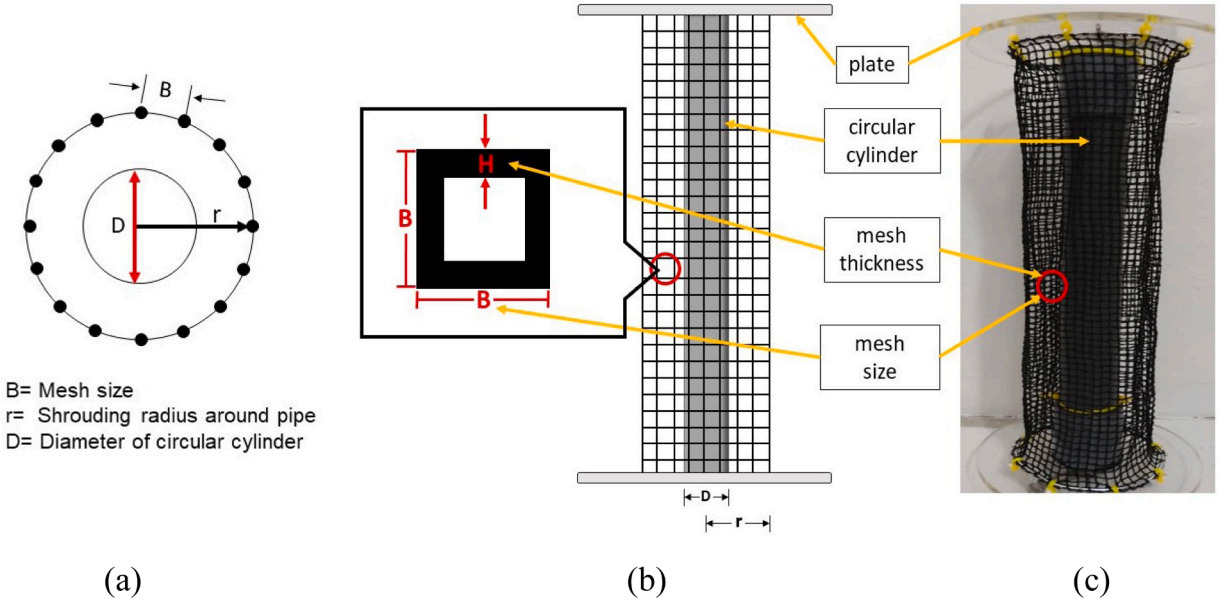


**Fig. 2.** Schematic diagram of the shroud (a) Top view (b) Side view (c) Cylinder fitted with shroud of $B = 0.2D$ $H = 0.03D$.

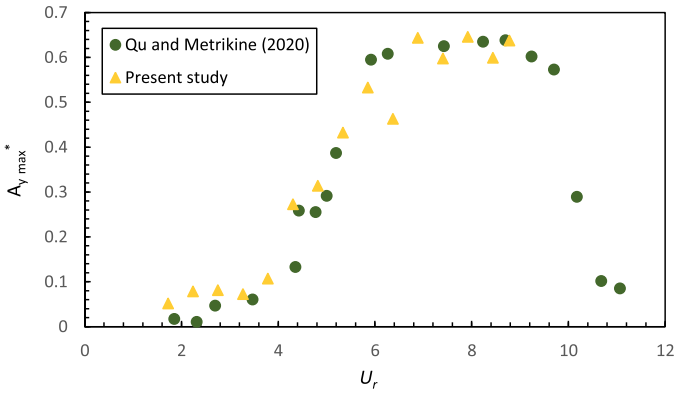


**Fig. 3.** Maximum CF Amplitude ratio of a bare cylinder.

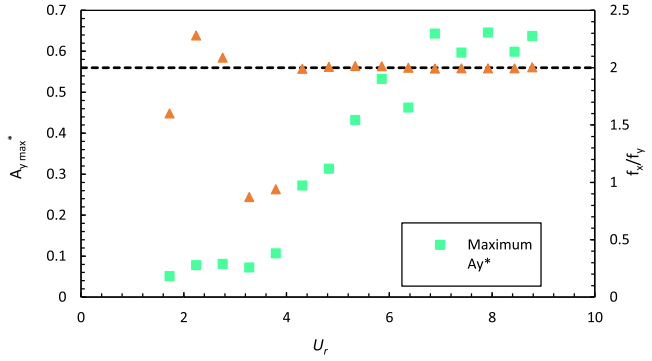


**Fig. 4.** IL and CF Frequency ratio ($f_x/f_y$) of a bare cylinder and Maximum CF Amplitude ratio ($A_{y\ max}$*) of a bare cylinder as a function of reduced velocity.

flexible cases, it can be noticed that a larger shroud radius would provide a better performance in suppressing VIV and $C_{d\ mean}$ and hence, lead to the decision of using $r = 1.3D$ as the shroud radius in the present study.

The shroud that surrounded the cylinder was flexible and in a square pattern, as shown in Fig. 2. Four different mesh sizes were proposed in order to identify the efficiency of the shroud. The dimensions of the

**Table 3**
Measurement uncertainty of the Free Decay Tests at Nahrim.

| Shroud configuration | Measurement uncertainty of amplitude response (%) | Measurement uncertainty of force measurement (%) |
|---|---|---|
| Bare | 2.30 | 0.33 |
| $B = 0.2D$ $H = 0.03D$ | 3.00 | 0.33 |
| $B = 0.4D$ $H = 0.03D$ | 1.40 | 0.33 |
| $B = 0.6D$ $H = 0.03D$ | 2.30 | 0.33 |
| $B = 0.8D$ $H = 0.03D$ | 4.00 | 0.33 |
| $B = 0.6D$ $H = 0.03D$ | 2.30 | 0.33 |
| $B = 0.6D$ $H = 0.09D$ | 4.60 | 0.33 |
| $B = 0.6D$ $H = 0.11D$ | 0.53 | 0.33 |

mesh size were obtained by referring to Kumar et al. (Kumar et al., 2018)'s and Huera-Huarte (Huera-Huarte, 2017)'s studies, since both of the studies have different outcomes on the optimum mesh size. On the other hand, investigations regarding mesh thickness (H) of the shroud are very limited as the addition of bobbins or tubes led to a gain in density. In the present study, instead of using external sources, the thickness of the shroud was used in differentiating mesh thickness because it is the most basic design with a low cost of fabrications. The thickness of the shroud was designed based on the theory of boundary layer thickness (Schlichting, 1968), as shown in Eq. (1):

$$V_L = \frac{y}{R}\sqrt{\frac{U_\infty}{\nu}} \tag{1}$$

Where $V_L$ is the boundary-layer velocity, and $R$, $U$ and $\nu$ denote the radius of the pipe, velocity, and kinematic viscosity, respectively. By referring to the boundary layer around a circular cylinder, the boundary layer thickness calculated was found to be $0.06D$. Therefore, a mesh with a lower thickness ($H = 0.03D$) and two with a larger thickness ($H = 0.09D$ and $0.11D$) were tested. The data were recorded for 60 s after the current flow achieved steady-state condition. The data obtained for cylinder vibration was ensured to be in stable conditions. Free decay test was conducted before starting the experiment for the bare cylinder as

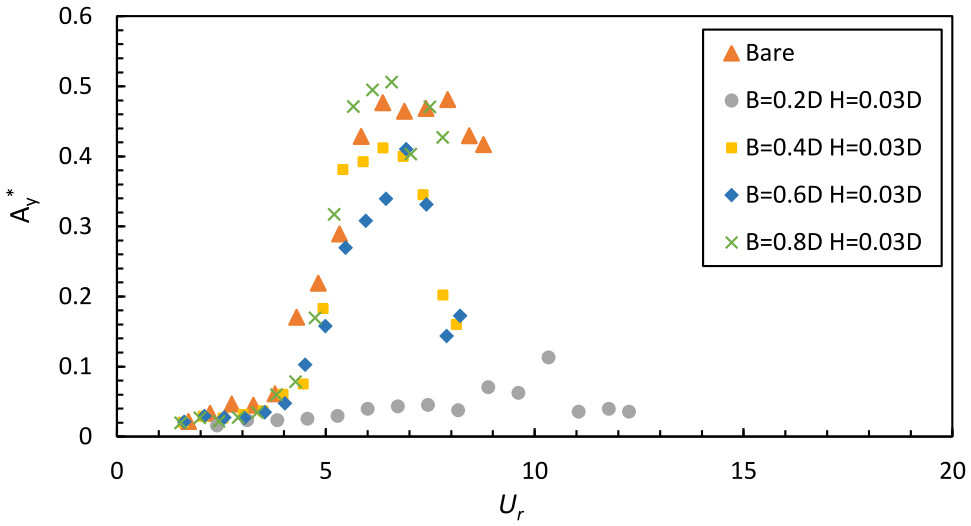


(a)

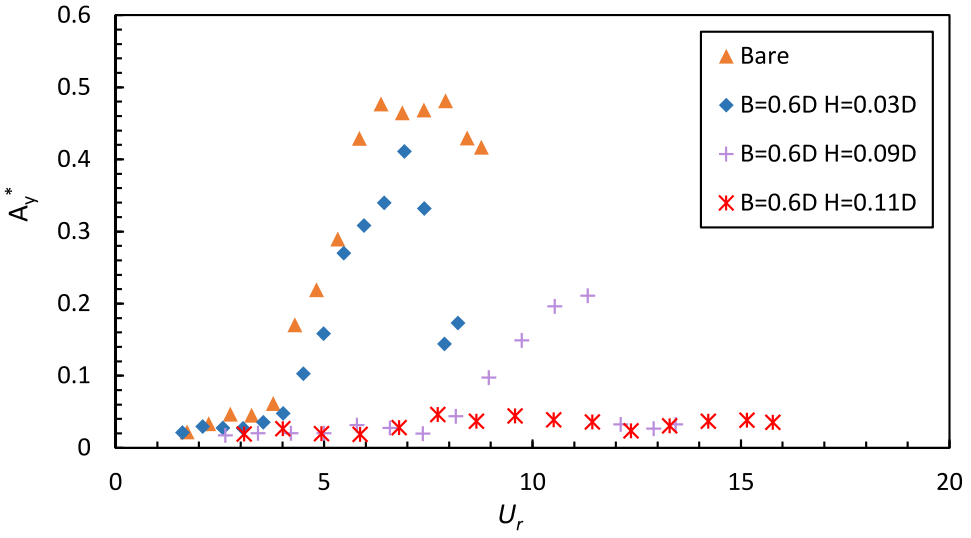


(b)

**Fig. 5.** CF amplitude ratio of a bare cylinder and cylinder fitted with different (a) Mesh size (b) Mesh thickness.

well as cylinders with shrouds in order to obtain the natural frequencies by pulling the cylinders downwards and allowing it to vibrate freely until it stops. The natural frequency ($f_n$) of the bare cylinder was 1.76 Hz in water. The natural frequencies of each cylinder with shrouds were in the range of 0.98 ~ 1.98. The values were slightly different from each other, since the mass of the cylinder with shrouds was different due to the additional mass of the shrouds.

### 2.3. Measuring equipment and test procedure

A tri-axial force sensor was used to measure the drag responses, as shown in Fig. 1. The force sensor was connected to the strain gauge amplifier and then to the laptop, so that the drag force in the time domain can be recorded for further analysis. The sampling frequency of the force sensor and camera are 1200 Hz and 60 fps, respectively. The camera was installed on the water flume wall which was located approximately 10 cm from the side of the strut. The strut and plate were made of transparent material allowing optical access to the camera to record the vibration amplitude in CF direction. The video data recorded by the camera was analysed using Tracker video analysis and modelling tools software. The frequency response is obtained by converting the amplitude response in the time domain into the frequency domain using the Fast Fourier Transform (FFT) as shown in Eq. (2):

$$A(r) = \pi \sum_{k=0}^{N-1} X(s) e^{-\frac{i2\pi}{N^2}}, r = 0,\ 1,\ 2,\ N-1 \quad (2)$$

Where *X(s)* is the periodic wake that is sampled at Nyquist Frequency or even higher, and *s* is the number of samples collected from the original signals.

## 3. Results and discussion

### 3.1. Validation of the study

To validate the present study, the existing experimental data of Qu and Metrikine (Qu and Metrikine, 2020) was used for comparison. The results were presented in terms of maximum CF amplitude ratio

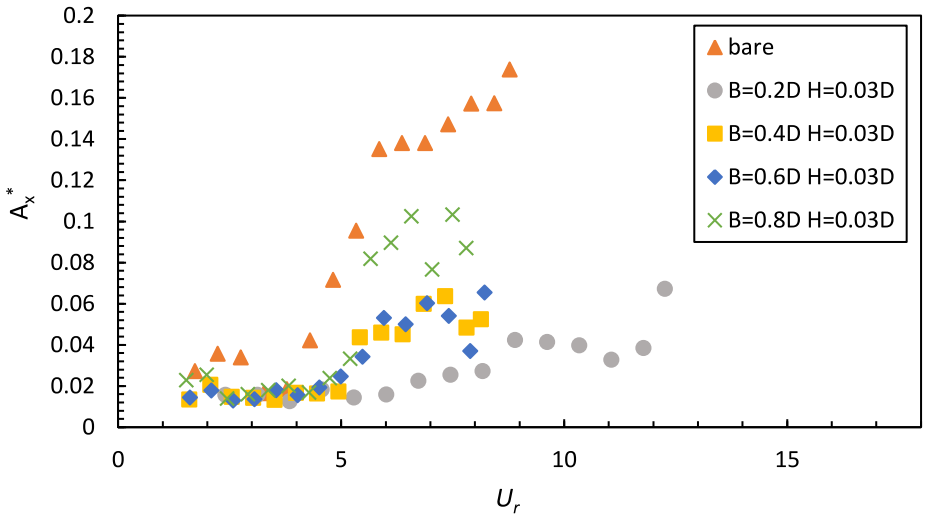


(a)

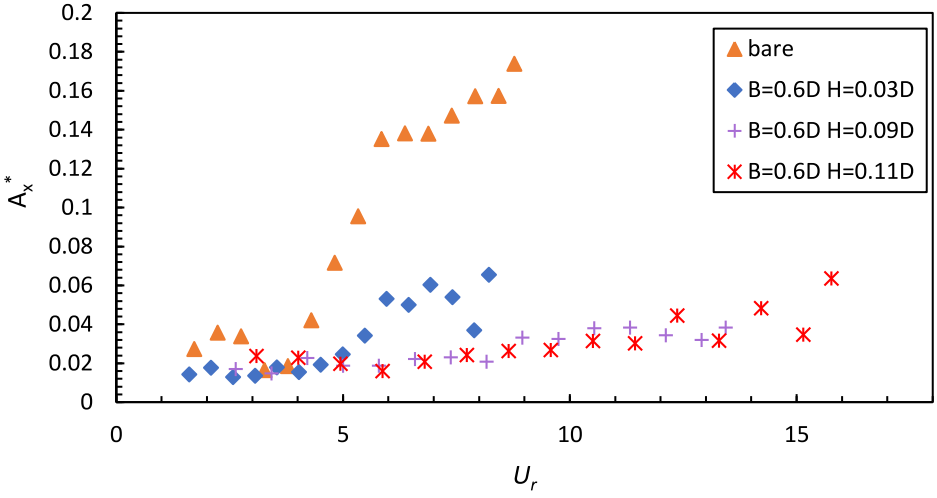


(b)

**Fig. 6.** IL amplitude ratio of a bare cylinder and cylinder fitted with different (a) Mesh size (b) Mesh thickness.

**Table 4**
The suppression effectiveness of the shroud based on CF amplitude reduction.

| Shroud configuration | The efficiency of CF amplitude reduction (%) |
|---|---|
| $B = 0.2D$ $H = 0.03D$ | 76.62 |
| $B = 0.4D$ $H = 0.03D$ | 14.41 |
| $B = 0.6D$ $H = 0.03D$ | 19.05 |
| $B = 0.8D$ $H = 0.03D$ | −5.20 |
| $B = 0.6D$ $H = 0.03D$ | 19.05 |
| $B = 0.6D$ $H = 0.09D$ | 56.62 |
| $B = 0.6D$ $H = 0.11D$ | 90.42 |

($A_{y\ max}{}^* = A_{y\ max}/D$) where $A_{y\ max}$ is the 10% of the highest peaks and $D$ is the diameter of the cylinder. The reduced velocity is defined as $U_r = U/f_n$D where $U_r$ was set from 2.0 to 9.0. Based on Fig. 3, the pattern and values of $A_{y\ max}{}^*$ obtained in the present study were in good agreement with Qu and Metrikine (Qu and Metrikine, 2020). It was found that at a reduced speed range of $2.0 < U_r < 4.3$, no significant indication of the VIV phenomenon is found. Meanwhile, an increment of amplitude response is observed in the reduced speed range of $4.3 < U_r < 7.9$. At $U_r \geq 7.9$, consistent high $A_{y\ max}{}^*$ values were found. This observation is in agreement with the research of Goncalves et al. (Gonçalves et al., 2013) as large-amplitude vibration or shedding frequency can lock in and shift to match the natural frequency within the range of ($2 < U_r < 12$). Due to the limitation of the water flume, the maximum $U_r$ that can be achieved by the present study is $U_r = 9$. However, the data of the present study is adequate as it covers the typical lock-in region of VIV, where in general, the range is reported from $5 < U_r < 8$ (Qu and Metrikine, 2020).

Meanwhile, Fig. 4 demonstrates the symbols of green square and orange triangle that represents the relationship between the maximum CF amplitude ratio and the IL-to-CF frequency ratio of bare cylinder at various reduced velocities, respectively. At lower reduced velocity that ranges from 2 to 4, the IL-to-CF frequency ratio changes due to the creation of irregular and unstable vortices in the cylinder's near wake. This indicates the absence of the VIV. Starting from $U_r = 4.3$, the vortex shedding becomes periodic, where the IL oscillating frequency is at twice the CF frequency. It is a well-known fact that the IL frequency response should be twice of CF frequency response for a bare cylinder.

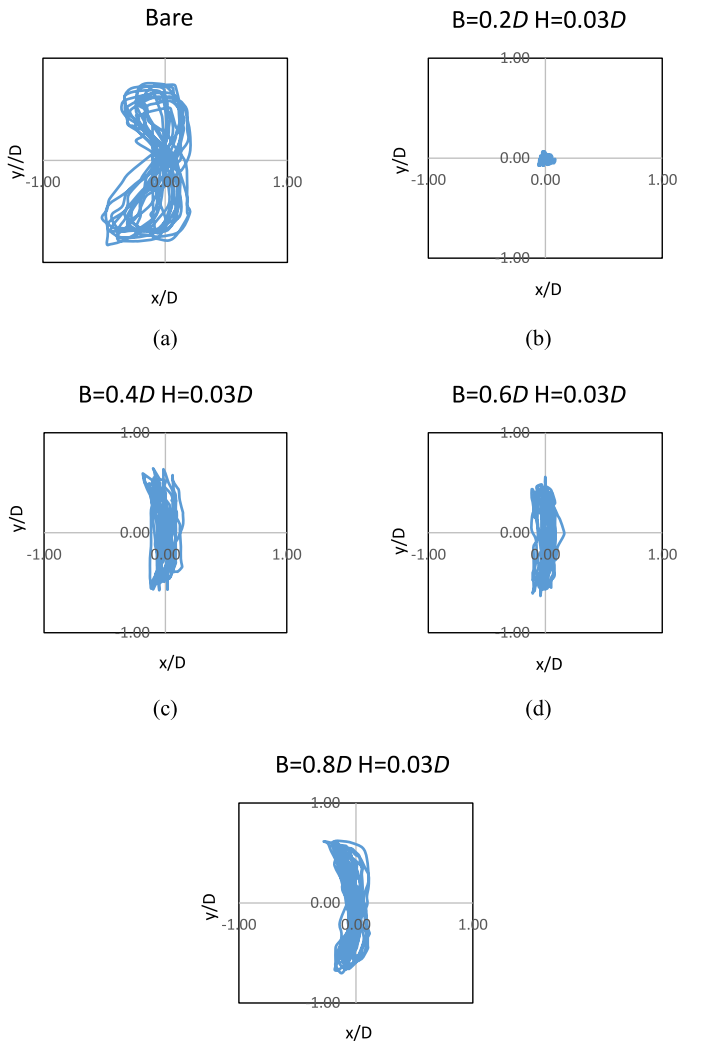


**Fig. 7.** Trajectory of a bare cylinder and cylinder fitted with different mesh size at $U = 0.46$ m/s: (a) Bare cylinder, (b) $B = 0.2D$ $H = 0.03D$, (c) $B = 0.4D$ $H = 0.03D$, (d) $B = 0.6D$ $H = 0.03D$, (e) $B = 0.8D$ $H = 0.03D$.

This is considered as the developing condition of VIV where the IL vibration is lock-on to the CF vibration with the ratio of 2. Therefore, it can be seen that the amplitude ratio starts to increase rapidly from $U_r = 4.3$.

Besides the validation based on amplitude response, random standard uncertainty is also used for measuring the uncertainty of amplitude and force measurements in the present study. The uncertainty evaluation is based on the Free Decay Test of the present study. Each case consists of 3 sets of repeated data. The $S_{\bar{x}}$ (random standard uncertainty) of the tests is calculated by (Eq. (3)):

$$S_{\bar{x}} = \frac{S_x}{\sqrt{N}} \tag{3}$$

where $S_x$ is the standard deviation of the repeated tests, divided by the square root of the number of observations (N). From the results presented in Table 3, force measurements are found to be very consistent with low uncertainty over different shroud configurations. It is because of the high sensitivity of the force sensors and precise calibration. As




**Fig. 8.** Trajectory of a bare cylinder and cylinder fitted with different mesh thickness at $U = 0.46$ m/s: (a) Bare cylinder, (b) $B = 0.6D$ $H = 0.03D$, (c) $B = 0.6D$ $H = 0.09D$ (d) $B = 0.6D$ $H = 0.11D$.

overall, all of the cases obtained are less than 5% for the uncertainty. In other words, the tests have low uncertainty as the value are less than 5% (Usta and Duranay, 2020). These results show the reliability a of the VIV tests conducted at the water flume of NAHRIM.

### 3.2. Vibration amplitude responses

In the discussion of the shroud performance, the responses of the bare cylinder in the present study are included as a basis of comparison. Fig. 5 and Fig. 6 indicate the vibration amplitude ratio of the bare cylinder and cylinder fitted with shroud having different mesh size (B) and mesh thickness (H) versus the reduced velocity in CF and IL directions, respectively. The amplitude ratio, $A_y{*}$ is defined as ($A_y/D$), meanwhile, $axe{*}$ is defined as ($axe/D$), where $A_y$ and $axe$ are the standard deviation of the displacement in CF and IL directions, respectively. $D$ is the diameter of a cylinder. $U_r$ is defined as $U/f_nD$ where $U$ is flow speed and $f_n$ is the natural frequencies of bare cylinder and shroud cases.

Based on Fig. 5(a), the highest amplitude ratio is found at $U_r$ =6.5 for cylinder fitted with shroud having $B = 0.8D$ and $H = 0.03D$, which is reported even higher than the bare cylinder. The synchronization occurs generally between $4.3 \leq U_r \leq 9$ for the VIV response of the bare cylinder. Overall, Fig. 5(a) shows that all shrouds managed to reduce peak amplitude of displacement within the synchronization range except for shroud with $B = 0.8D$ and $H = 0.03D$. The shroud having a mesh size smaller than $B = 0.4D$ had a better suppression performance. The change in mesh size is also able to narrow the lock-in range, which can obviously be seen in the shroud having $B = 0.2D$ to $0.6D$.

Table 4 shows the suppression effectiveness of the shroud, where it can be calculated as follows (Eq. (4)):

$$Efficiency\,(\%) = \frac{\left(A_{y\,highest}{}^{*}\right) bare\ cylinder - \left(A_{y\,highest}{}^{*}\right) cylinder\ fitted\ with\ shroud}{\left(A_{y\,highest}{}^{*}\right) bare\ cylinder} \times 100\% \tag{4}$$

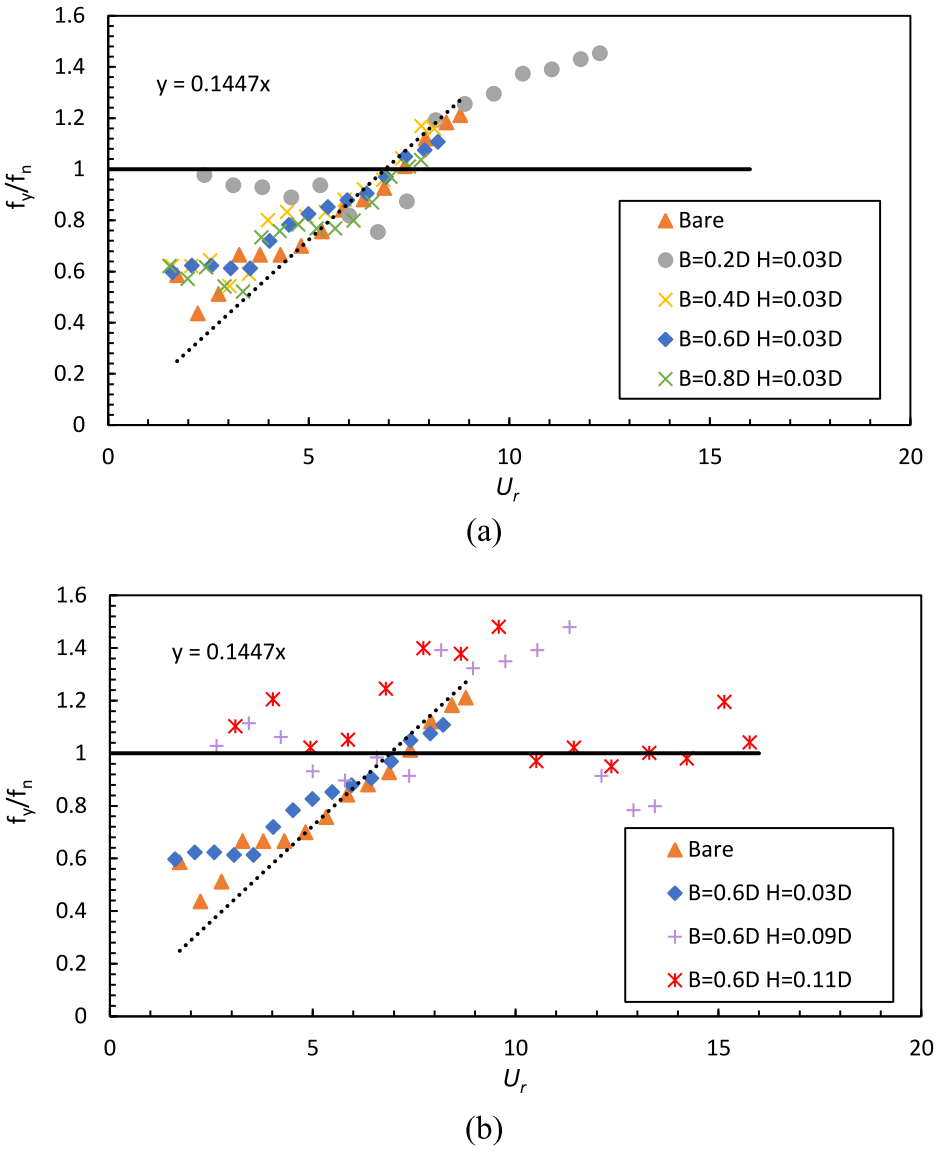


**Fig. 9.** CF frequency ratio of a bare cylinder and cylinder fitted with different (a) Mesh size (b) Mesh thickness.

Where $A_{y\ highest}$ * is referring to the highest value of CF amplitude ratio. Based on Table 4, shroud having $B = 0.2D$ $H = 0.03D$ reached a maximum amplitude of $A_y^* \approx 0.1$, accounting for a 76.62% reduction when compared to the peak amplitude of bare cylinder. It shows that shroud having $B = 0.2D$ $H = 0.03D$ is able to attenuate the vortex-induced vibration efficiently. This condition is consistent with Brown and King (Brown et al., 2008) who asserted that the net substructure or shrouds significantly impair the vortex shedding mechanism by interfering with the flow separation process. It is a well-known fact that due to the shear forces, the boundary layer will eventually break from a circular cylinder structure and generate vortex. If the vortex formed around the pipe is not symmetrical, VIV is generated as a result of the changing pressure distribution on the cylindrical structure's surface. The presence of shroud is able to disrupt the occurrence of the boundary layer separation and hence modify the formation of wakes behind the structure (Huera-Huarte, 2017).

According to Fig. 5(b), the highest amplitude of the bare cylinder is about 0.48, occurred at $U_r = 7$, which is within the consensus range found in the Sumer and Fredsoe (Sumer and Fredsoe, 1997). By increasing the mesh thickness, the amplitude ratio is decreasing. To further justify the reduction of amplitude due to the mesh thickness, the boundary layer's thickness is taken as a reference. The thickness of the boundary layer for a cylinder is found to be around $0.06D$ based on the theoretical calculation (1). Hence, mesh thickness with $H = 0.09D$ is assumed to be adequate to disrupt the flow boundary layer and to greatly reduce the amplitude of vibration. In fact, as illustrated in Fig. 5 (b), the shroud having $B = 0.6D$ and $H = 0.09D$ can achieve up to 56.62% in amplitude reduction, which is 37.57% higher than $H = 0.03D$. Based on Table 4, shroud with $H = 0.03D$ can merely reduce 19.05% of the amplitude ratio. Shroud having $B = 0.6D$ $H = 0.11D$ shows an excellent performance in suppressing the amplitude by 90.42%.

Fig. 6 shows that the IL amplitude ratio presents local maxima at $U_r$= 2.2, followed by smaller values around the reduced velocity of 3.7 and an increase in peak amplitudes for larger $U_r$ values, exactly in the same range as the peak amplitudes of the CF direction. At $U_r$=8.7, the highest amplitude ratio of the bare cylinder is found. Overall, the amplitude responses of shrouds are smaller than the bare cylinder. It shows all shrouds with different mesh sizes and mesh thickness successfully attenuated the vibration amplitude in terms of IL direction. When comparing the CF and IL amplitude ratio, the IL amplitude ratio is significantly smaller than the CF amplitude ratio, whereby it is about 64% lower than the CF response. Hence, the CF amplitude response is

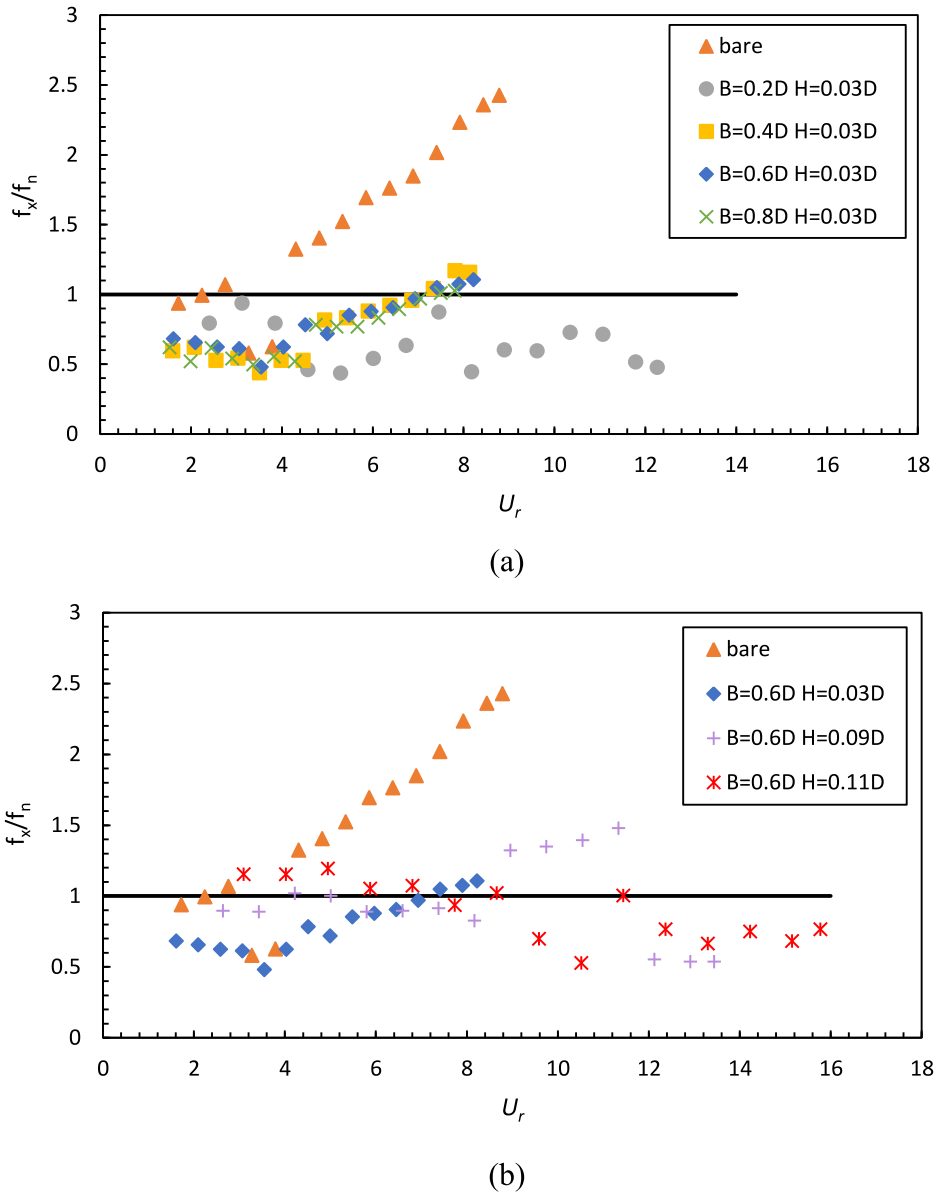


**Fig. 10.** IL frequency ratio of a bare cylinder and cylinder fitted with different (a) Mesh size (b) Mesh thickness.

found to be more critical as compared to the IL response. This is because of the well-organized vortex wake behind the cylinder, which generates different lift forces on each side, resulting in motion transverse to the flow. The shroud having $B = 0.2D$ and $H = 0.03D$ managed to keep good performance in both directions. Meanwhile, Fig. 6(b) shows shroud with the highest mesh thickness $B = 0.6D$ and $H = 0.11D$ is able to reduce IL vibration amplitude in the CF direction.

To have a better understanding of the vibration amplitude, the trajectory of the cylinder fitted with shroud of different mesh sizes and mesh thickness are shown in Figs. 7 and 8, respectively. The uniform velocity flows from left to right in the figure. The trajectory of the circular cylinder cross-section model under the test conditions is shown by taking the IL and CF displacement of the cylinder simultaneously. The X-axis in the figures indicates the IL displacement, while Y-axis shows the CF displacement. Based on Fig. 7, a well-known "8″-shaped locus is observed, where a similar outcome was also reported by Senga et al. (Senga et al., 2018). As it can be seen in Fig. 7(b), a shroud with $B = 0.2D$ and $H = 0.03D$ is able to suppress vibration in IL as well as CF directions as compared to the trajectory of the bare cylinder. Only small displacements are shown in both directions. The trajectory for a shroud of $B = 0.4D$ and $B = 0.6D$ is similar, where the IL displacement is smaller as compared to CF displacement. When comparing the mesh thickness in Fig. 8, the shroud having $B = 0.6D$ and $H = 0.11D$ has shown the smallest displacement in the CF direction (Fig. 8(d)).

### 3.3. Frequency responses

The frequency response is obtained using FFT to convert the time domain data into a frequency domain. Previous researchers have mentioned the phenomenon of lock-in region by explaining that the "synchronization" occurs when the frequency of vortex shedding is equal or becomes close to the natural frequency of the structure. The shedding frequency and the oscillation frequency remain close to the natural frequency of the structure, and thus the frequency ratio remains close to unity (Brown et al., 2008). The dashed line in Fig. 9 is the fitted line plot for Strouhal number. As reported by Summer and Fredsoe (Sumer and Fredsoe, 1997), the value of the Strouhal number is around 0.2 to 0.21. Due to the low aspect ratio of the present study, the Strouhal number is smaller than 0.2, which is 0.1447. This is in agreement with Park et al. (Park and Lee, 2002), where $St$=0.14 was obtained from their

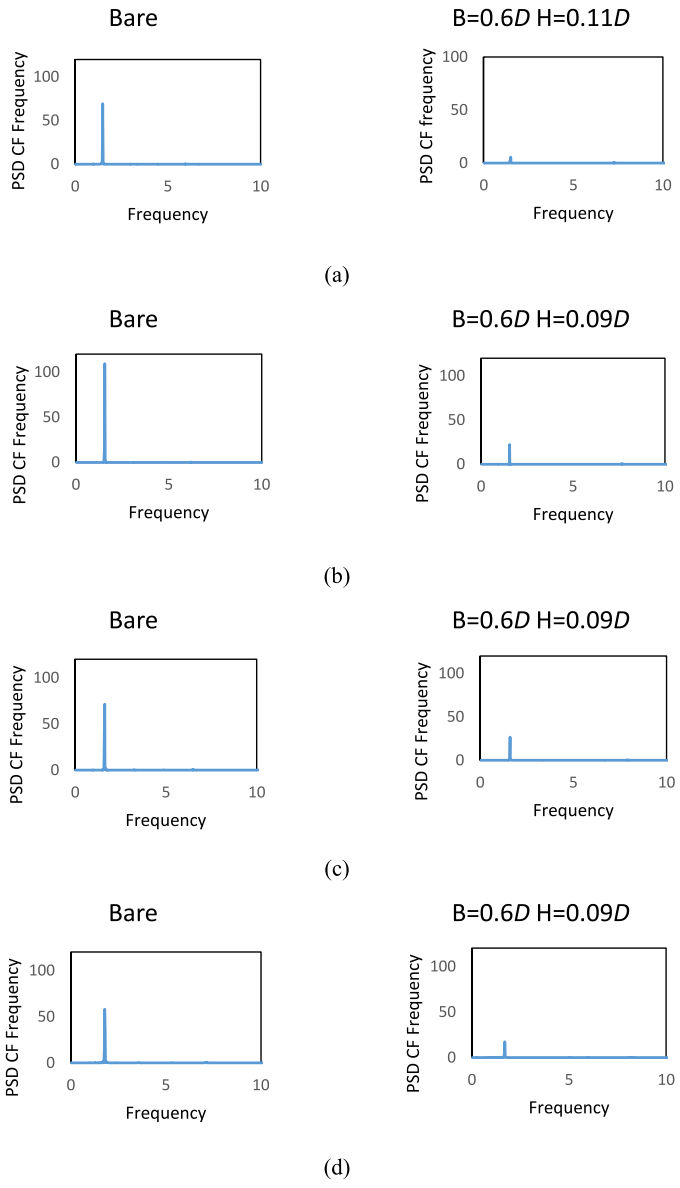


**Fig. 11.** Comparison of the PSD of bare cylinder and cylinder with shroud $B = 0.6D$ $H = 0.09D$ at different speeds: (a) 0.34 m/s, (b) 0.37 m/s, (c) 0.40 m/s, (d) 0.46 m/s.

experiment. According to Katopodes (Katopodes, 2018), a high Strouhal number represents the domination of oscillation in the flow, while low Strouhal number indicates the oscillations are swept by the speeding flow. In our case, due to the low mass ratio of the cylinder, the Strouhal number is slightly lower, and hence the domination of the vortex shedding frequency is expected to be lesser compared to high mass ratio cylinder.

The black line in Figs. 9 and 10 is known as the synchronization line ($f^* = 1$), indicating that the CF frequency and IL frequency are the same as that of the natural frequency ($f_n$) of the elastically mounted cylinder and the shrouds. As it can be seen in Figs. 9 and 10, the frequency ratio of the bare cylinder is not precisely equal to unity during the lock-in region. This "nonclassical" behaviour of frequency ratio occurred because of imposing a low mass ratio. This can be supported by Khalak et al. (Khalak and Williamson, 1999), whereby it has been stated that the classic scenario was only applicable for a large mass ratio. A similar dynamic phenomenon is also shown in previous studies (Qu and Metrikine, 2020), (Park and Lee, 2002; Katopodes, 2018; Khalak and Williamson, 1999; Khalak and Williamson, 1997). Jason Tranter explained that the resonance will cause all the vibrations within approximately 20% of the natural frequency to be amplified (Tranter, 2015). Goncalves et al. (Gonçalves et al., 2013) reported that the case of $m^* = 1$ is extremely relevant for offshore applications. From the observation, all shrouds except for the one with $B = 0.2D$ and $H = 0.03D$ are following the expected Strouhal frequency at all reduced velocities as shown in Fig. 9(a). On the other hand, Fig. 9(b) reveals that shroud having $B = 0.6D$ $H = 0.09D$ and $B = 0.6D$ $H = 0.11D$ successfully disrupted the shear layer that was generated behind the cylinder as both cases are not following the vortex shedding line. In fact, the frequencies of both cases are scattered around without any specific pattern. This can be explained further in Fig. 11 by referring to their power spectral density (PSD) in the CF direction.

Fig. 11 demonstrates the intensity difference of both cases which are bare cylinder and cylinder fitted with a shroud of $B = 0.6D$ $H = 0.09D$. Shroud having $B = 0.6D$ $H = 0.09D$ shows smaller intensity with the frequencies scattering around from 1, not lock-in into the natural frequency. This proves that the shroud is able to modify the wake formation mechanisms and disrupt the lock-in of the frequencies, and hence attenuates the amplitude responses. It can be observed in Fig. 11(d), that a significant PSD peak of the bare cylinder occurs during the lock-in condition ($U_r = 7.9$), while the PSD peak of the shroud having $B = 0.6D$ and $H = 0.09D$ is lower as compared to that of a similar speed velocity.

In Fig. 10, the IL frequencies of the bare cylinder are found to vibrate at higher mode, which is about two times higher than the CF frequencies response. In fact, by referring to Fig. 12, the frequency ratio between IL to CF is found to be 2 for the bare cylinder. It is in agreement with Goncalves et al. (Gonçalves et al., 2013) under the VIV phenomenon. After implementing the shroud, the vibrating frequency in the IL direction has reduced significantly, where higher mode vibration is undetectable. The IL to CF frequencies ratio of the shrouds is noticed to be close to 1 in most of the cases (Fig. 12), indicating that the shroud is able to suppress the higher mode of vibration. Besides, it is interesting to find that there is no consistent ratio for shroud with $B = 0.2D$ $H = 0.03D$, $B = 0.6D$ $H = 0.09D$ and $B = 0.6D$ $H = 0.11D$, indicating that the typical VIV response has been totally disrupted by these shrouds.

In order to further explain the VIV phenomenon in detail, the PSD together with the time series vibration of all shrouds with different mesh sizes and thickness in CF direction are presented in Figs. 13 and 14, respectively. For the time series amplitude response, it is extracted at a speed of 0.51 m/s for all the cases for a duration of 6 s after the cylinders achieve steady vibration. A dotted reference line is plotted for all the plots for ease of comparison.

Based on Fig. 13, it can be seen that the PSD of the bare cylinder and cylinder fitted with shroud having $B = 0.8D$ $H = 0.03D$ are high. For the bare cylinder, the intensity of PSD increases as the reduced velocity increases. The highest intensity is found at higher $U_r$. Although the shroud with $B = 0.8D$ $H = 0.03D$ is having high PSD, it is able to reduce the intensity at high reduced velocity as shown in Fig. 13(b). It indicates that this shroud is able to cut down the vibration intensity of a bare cylinder at a higher $U_r$. Other mesh sizes and thickness are able to further reduce the PSD intensity to much lower values. It is worth noting that the PSD intensity of shroud having $B = 0.2D$ $H = 0.03D$ and $B = 0.6D$ $H = 0.11D$ are extremely low as compared to other cases. By referring to the time series (Fig. 14(d)) vibration amplitude, both cases display merely small vibrations. It shows that both cases are successful in suppressing both the vibration amplitude as well as the intensity of the cylinder.

In summary, a strong coupling between CF and IL motions is presented for the bare cylinder according to Fig. 4. Indeed, by inspecting the results in Figs. 5 and 6, three steady regimes that can be observed. The first at a reduced velocity of 2, is featured by predominantly IL oscillation with a small CF oscillation (Fig. 6). On the other hand, an opposite behaviour can be seen at a reduced velocity of 3, which is clearly featured by the dominant presence of CF oscillations. Once again, for

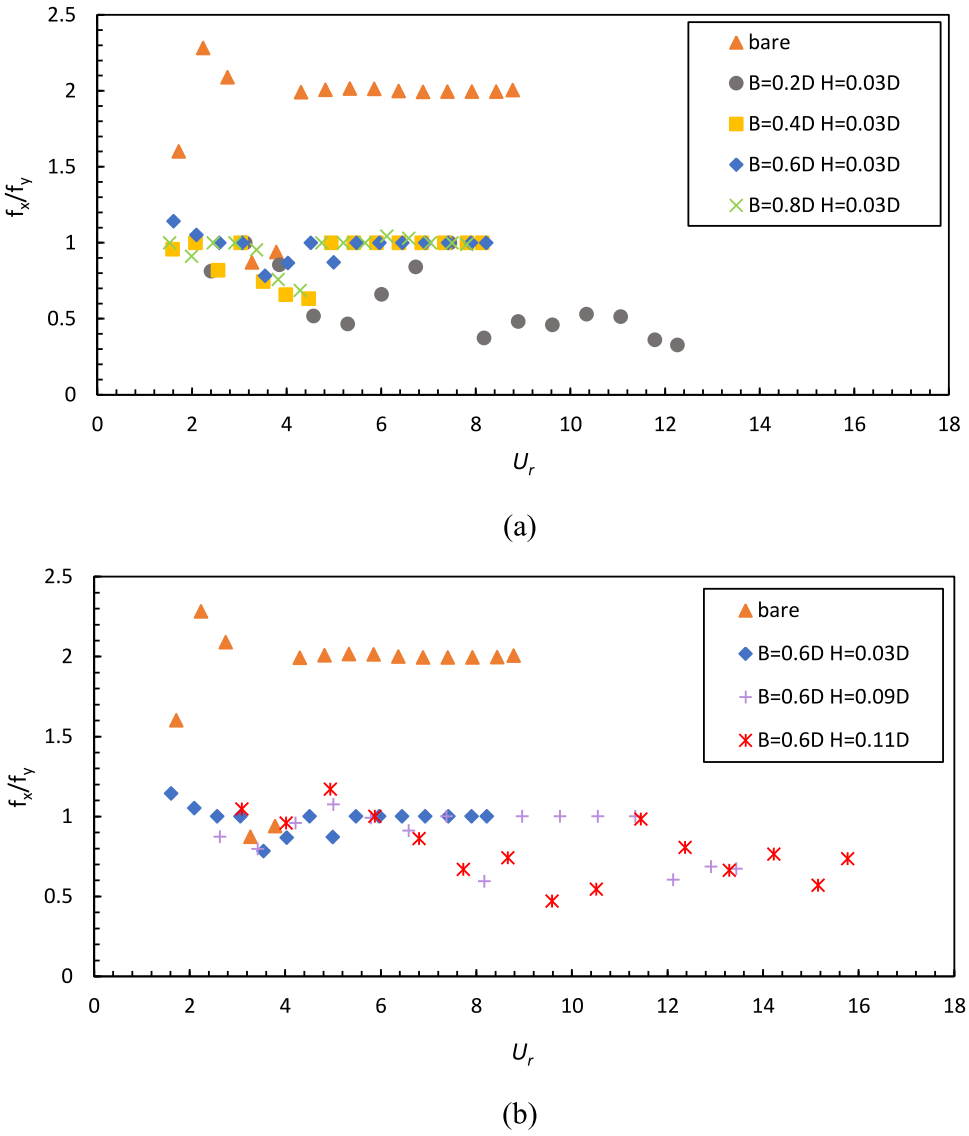


**Fig. 12.** IL to CF frequency ratio of a bare cylinder and cylinder fitted with different: (a) Mesh size (b) Mesh thickness.

reduced velocities higher than 4, a coupled movement starts, resulting in a notable increase of the oscillation in both directions and a ratio of two between the IL and CF motion frequencies. However, the condition changes as the shrouds are fitted around the bare cylinder. The IL-to-CF ratio of all configurations of the cylinder fitted with shrouds in Fig. 12 shows the value of one throughout the synchronization ($4.3 < U_r < 9$). This demonstrates that the shrouds are able to suppress the high mode vibration during lock-in where both IL and CF responses are in the same frequency. This can be supported by referring to their trajectories in Figs. 7 and 8. As it can be observed in both Figures, the 8 shape trajectories were totally removed by the shrouds. It can be clearly seen in Fig. 7(b), where shroud having $B = 0.2D$ and $H = 0.03D$ only produces the small shape trajectory. This has proven that all shrouds except $B = 0.8D$ and $H = 0.03D$ are able to suppress the typical VIV phenomenon.

### 3.4. Mean drag coefficient

Mean drag coefficient ($C_{d\ mean}$) is one of the important characteristics that need to be addressed in evaluating the performance of suppression devices. The mean drag coefficient is identified as $C_{d\ mean} = \frac{F_{d\ mean}}{\frac{1}{2}\rho u^2 LD}$. $F_{d\ mean}$ represents mean drag force and $\rho$, $U$, $L$ and $D$ are denoted as density, flow velocity, length of the cylinder, and diameter of the cylinder, respectively.

The $C_{d\ mean}$ of a bare cylinder and cylinder fitted with shroud having different mesh sizes and mesh thickness are identified in the Figs. 15(a) and 15(b), respectively. Table 5, on the other hand, shows the average $C_{d\ mean}$ of the cylinders with various shroud configurations and its reduction efficiency. Based on Fig. 15(a), the $C_{d\ mean}$ of the bare cylinder increases gradually as the $U_r$ increases. The $C_{d\ mean}$ displays a significant jump at $U_r \approx 4$, which corresponds to the high amplitude ratio jump at the same $U_r$ in Fig. 5(a). This condition is in agreement with Quen et al. (Quen et al., 2018), where the amplification of the amplitude in the lock-in region magnifies the $C_{d\ mean}$.

The application of shrouds showed a reduction of the $C_{d\ mean}$ throughout the entire reduced velocities range. Based on Fig. 13, although a slight increment of $C_{d\ mean}$ values is found at the lock-in region, the shrouds of various mesh sizes (Fig. 15(a)) are still able to reduce $C_{d\ mean}$ as compared to the bare cylinder. The lower the mesh size, the higher the $C_{d\ mean}$ reduction, as shown in Table 5. The highest $C_{d\ mean}$ reduction that can be achieved by shroud having various mesh sizes is 48.4% for shroud of $B = 0.2D$ $H = 0.03D$. It is interesting to find that shroud having $B = 0.8D$ and $H = 0.03D$ is able to reduce the $C_{d\ mean}$ by 21.35% even though it is unable to attenuate vibration amplitude. It shows that the use of shroud can definitely reduce the $C_{d\ mean}$ although it

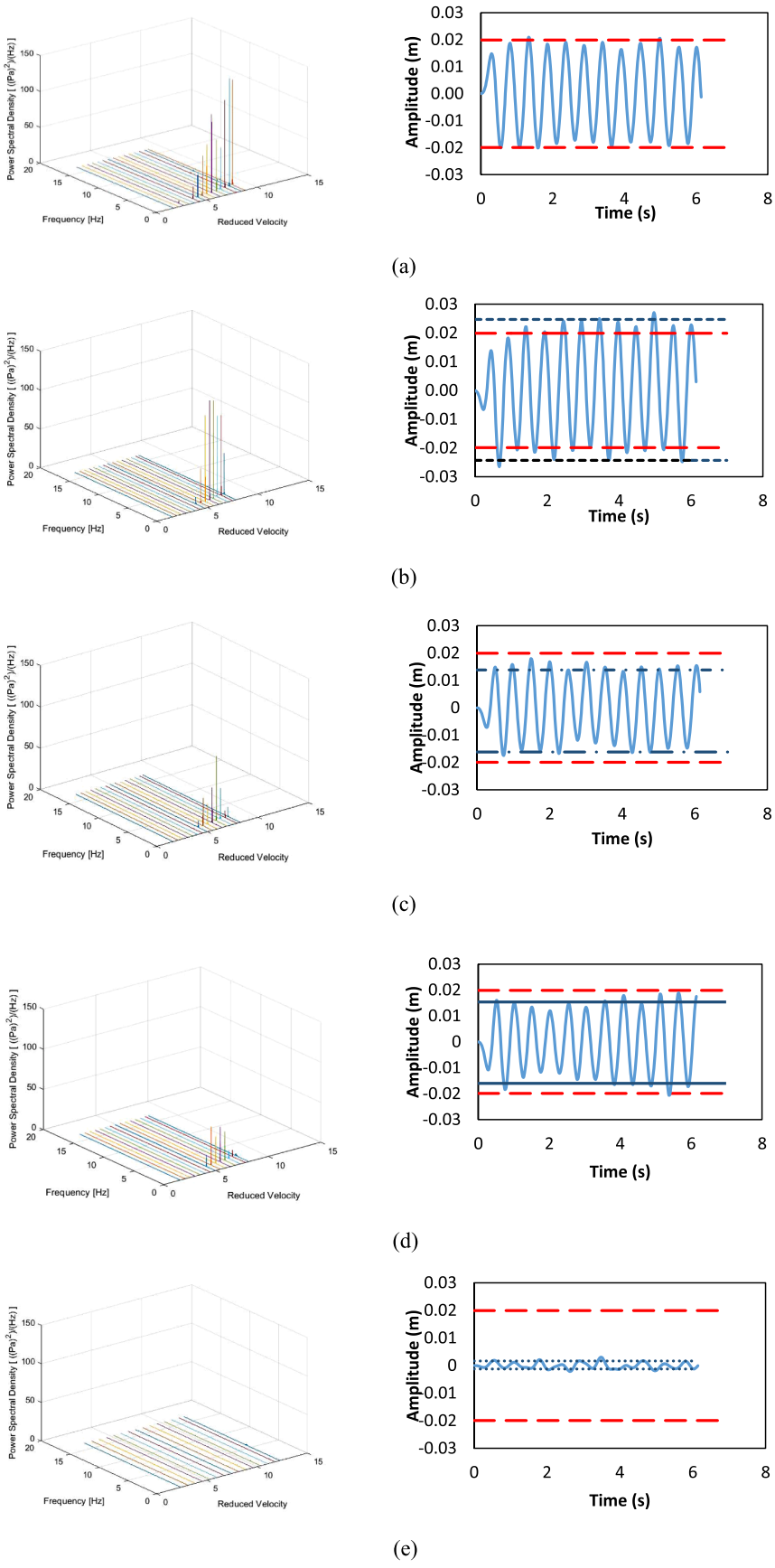


**Fig. 13.** The PSD and time series of bare cylinder and cylinder fitted with different mesh size at $U = 0.51$ m/s: (a) Bare cylinder, (b) $B = 0.8D$ $H = 0.03D$, (c) $B = 0.6D$ $H = 0.03D$, (d) $B = 0.4D$ $H = 0.03D$, (e) $B = 0.2D$ $H = 0.03D$. The red dotted line indicates the reference line for bare cylinder amplitude response while the blue dotted line represents the reference lines for cylinder fitted with shrouds.

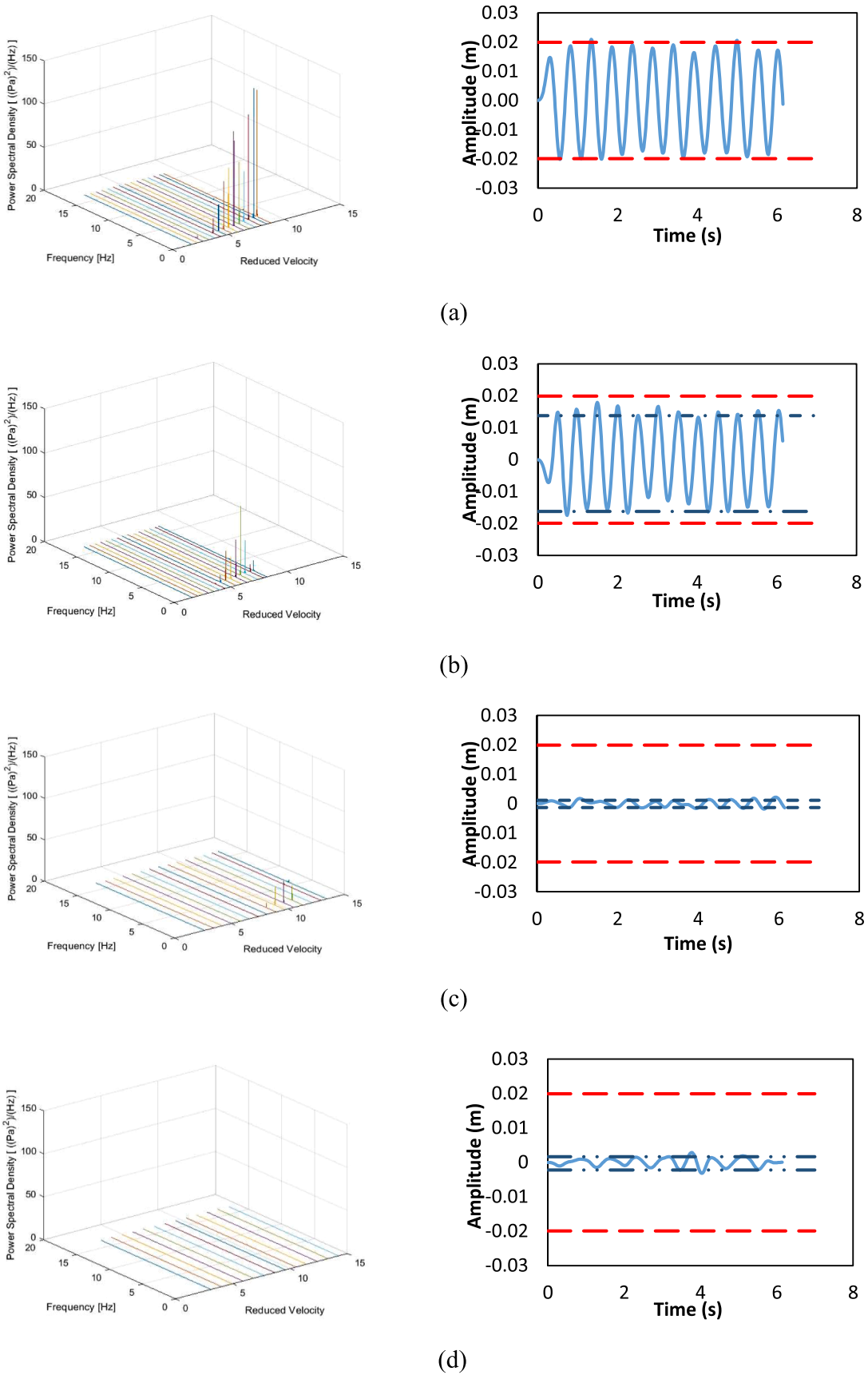


**Fig. 14.** The PSD and time series of bare cylinder and cylinder fitted with different mesh thickness at $U = 0.51$ m/s: (a) Bare cylinder, (b) $B = 0.6D$ $H = 0.03D$, (c) $B = 0.6D$ $H = 0.09D$, (d) $B = 0.6D$ $H = 0.11D$. The red dotted line indicates the reference line for bare cylinder amplitude response while the blue dotted line represents the reference lines for cylinder fitted with shrouds.

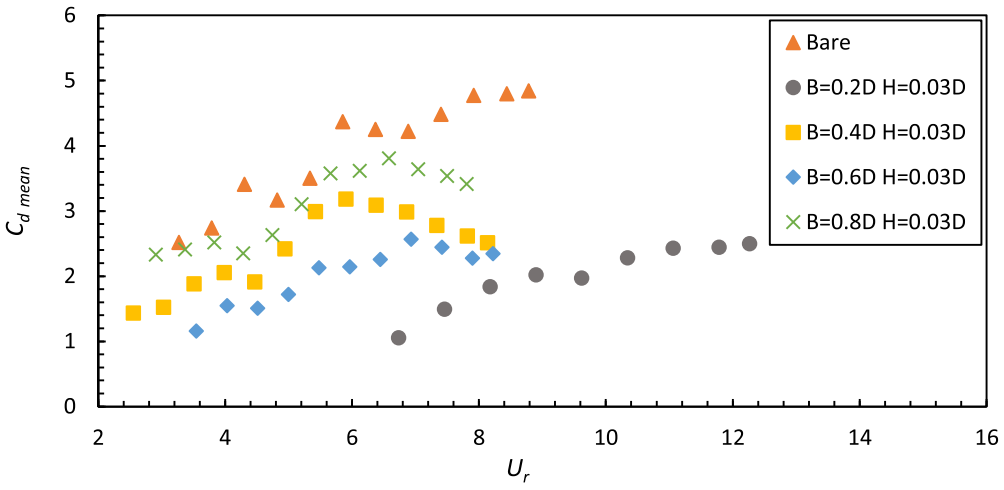


(a)

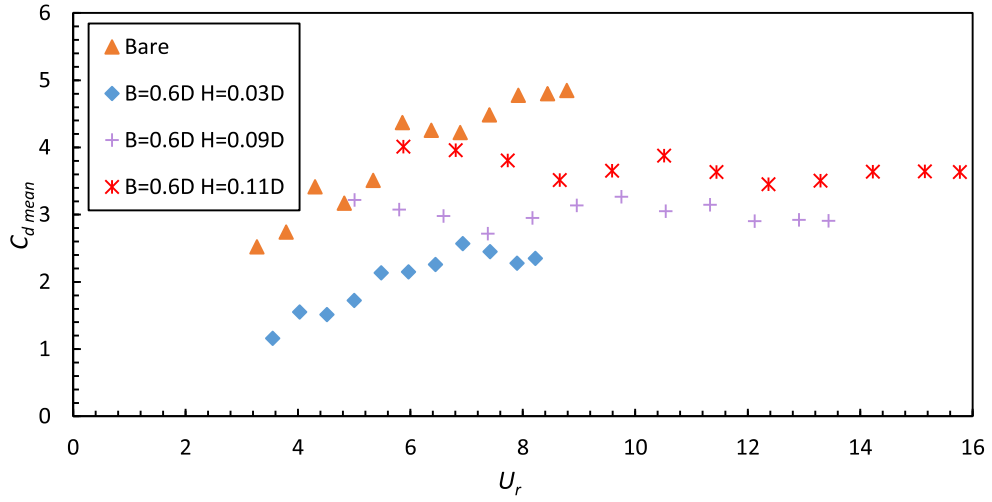


(b)

**Fig. 15.** The mean drag coefficient of a bare cylinder and cylinder fitted with different (a) Mesh size (b) Mesh thickness.

**Table 5**
Average $C_{d\ mean}$ of cylinders with various shroud configurations.

| Shroud configuration | $C_{d\ mean}$ | The efficiency of $C_{d\ mean}$ (%) |
|---|---|---|
| Bare | 3.925 | – |
| $B = 0.2D$ $H = 0.03D$ | 2.006 | 48.400 |
| $B = 0.4D$ $H = 0.03D$ | 2.416 | 34.290 |
| $B = 0.6D$ $H = 0.03D$ | 2.011 | 47.020 |
| $B = 0.8D$ $H = 0.03D$ | 3.080 | 21.350 |
| $B = 0.6D$ $H = 0.03D$ | 2.011 | 47.020 |
| $B = 0.6D$ $H = 0.09D$ | 3.022 | 32.600 |
| $B = 0.6D$ $H = 0.11D$ | 3.693 | 17.200 |

may not perform well in reducing the amplitude. The reduction of $C_{d\ mean}$ may be due to fluid entrainment that occurs within the shroud and flows out into the near-wake region. The entrainment of the flow increases the base pressure and hence reduces $C_{d\ mean}$ (M.M. Cicolin and Assi, 2017).

On the other hand, the change in mesh thickness ($H = 0.09D$ and $H = 0.11D$) is able to remain the $C_{d\ mean}$ value steadily without any increment during the typical lock-in region. It is corresponding to the amplitude response where the amplitude ratio for shroud with $H = 0.09D$ and $H = 0.11D$ are considerately lower as compared to other shrouds. In fact, for shroud with $H = 0.11D$, the amplitude ratio in the lock-in region is totally suppressed, with no significant peak. However, the $C_{d\ mean}$ reduction of shroud $B = 0.6D$ and $H = 0.11D$ is lesser as compared to the other configurations. It may be due to the higher contact surface (cross-sectional area) of the shroud for larger mesh thickness. Therefore, it results in a stronger $C_{d\ mean}$. Nevertheless, this is only an assumption that need to be further clarified through visualization and wake analysis. Although the shroud having $B = 0.6D$ and $H = 0.03D$ is less effective in suppressing amplitude responses as compared to $H = 0.11D$, it shows great performance in suppressing $C_{d\ mean}$ by 47.02% reduction. This is in contrast with the previous discussion in Fig. 5(b), where the shroud with the highest mesh thickness performs better in reducing vibration amplitude. It can be concluded that a lower mesh thickness produces a lower $C_{d\ mean}$.

The change of mesh thickness also results in a change of the mass ratio. However, it is assumed that the effect of the mass ratio is negligible compared to the effect of the thickness. As evidence, Cicolin and Assi (M.M. Cicolin and Assi, 2017) have been investigated $C_{d\ mean}$ of a thick-sparse mesh and thin-sparse mesh, with similar mass ratio (2.9 and

2.8 respectively). In their study, significant $C_{d\ mean}$ reduction has been noticed in thin-sparse mesh although similar mass ratio has been reported. Therefore, it is presumed that the mesh thickness has a much stronger impact on the shroud performance. To quantitatively evaluate the influence of shroud thickness on the $C_{d\ mean}$ of the present study, it is noticed the shroud with $H = 0.09$D reduces the $C_{d\ mean}$ by up to 32.6%, which is 15.4% more than the shroud with $H = 0.11$D.

Overall, all of the shrouds (except the one with $B = 0.8D$ $H = 0.03D$) are able to suppress VIV with various effectiveness. In terms of $C_{d\ mean}$ reduction, all shrouds have successfully reduced the $C_{d\ mean}$. In deciding the optimum parameters based on the present study, shroud having $B = 0.2D$ and $H = 0.03D$ is chosen as the main concern of VIV is to reduce both the vibration and $C_{d\ mean}$ of the structures. For shroud having $B = 0.2D$ and $H = 0.03D$, it is able to reduce 76.62% of vibration amplitude and 48.4% of $C_{d\ mean}$, which is much higher as compared to the shroud design of previous. Hence, an improvement is obtained in this present study.

Although the proposed configuration performs well in reducing VIV and $C_{d\ mean}$ compared to a bare cylinder, the two crucial parameters, mesh size and thickness, are not optimized at this time. Further research using a numerical scheme is required for the optimization of the essential parameters. In terms of shroud performance, only the behaviour of the shroud has been observed, not the behaviour of the cylinder. As a result, this is the study's drawback, and it may represent a future research gap.

The contribution of the present study is to improve shroud performance by altering mesh size and mesh thickness, which has the potential to reduce VIV and $C_{d\ mean}$. This innovative concept is able to achieve an optimum condition that is able to decrease the amplitude response without increasing $C_{d\ mean}$. In addition, this basic design is able to reduce $C_{d\ mean}$ better as compared to previous research. However, in terms of the practical application, the minimum mesh size will be determined by a variety of constraints, such as the clogging of shroud and the possibility of fabrication. It is hoped that by improving the suppression effectiveness, its potential application in the offshore industries can be implemented in the future.

## 4. Conclusions

In this study, an experiment analysis has been performed in a water flume to analyse the effect of VIV with different shroud variables. The amplitude, frequency, mean drag coefficient responses have been obtained for data analysis. The objectives of this research have been successfully achieved. From the experiment, the VIV effect has been successfully simulated on the circular rigid cylinder. The lock-in region was found at a reduced velocity ranging from $4.3 < U_R < 9$. Based on the present study, the frequency ratio of the bare cylinder during lock-in is not precisely equal to unity. This "nonclassical" behaviour of frequency ratio occurred due to a low mass ratio.

Then, the effectiveness of shrouds with different mesh sizes and mesh thickness in suppressing VIV of the short rigid cylinders was observed. For shrouds with different mesh sizes, all cases except for shroud having $B = 0.8D$ $H = 0.03D$ showed the capability to suppress VIV at different levels. The shroud having a mesh size smaller than $B = 0.4D$ had a better performance in suppressing the VIV of a short rigid cylinder. For shroud with different mesh thickness, all cases successfully attenuated the VIV. It is found that up to 90.42% of amplitude reduction can be achieved by the shroud having $B = 0.6D$ and $H = 0.11D$.

Meanwhile, the best $C_{d\ mean}$ reduction is found for shroud with $B = 0.2D$ and $H = 0.03D$ having 48.4% of suppression efficiency. The most effective shroud configuration by considering the suppression of amplitude and $C_{d\ mean}$ is shroud having $B = 0.2D$ and $H = 0.03D$, with 76.62% of amplitude reduction and 48.4% $C_{d\ mean}$ reduction.

## Declaration of Competing Interest

The authors declare that they have no known competing financial interests or personal relationships that could have appeared to influence the work reported in this paper.

## Acknowledgments

This work was financially supported by the Ministry of Higher Education Malaysia under Fundamental Research Grant Scheme, FRGS/1/2020/TK0/UTM/02/78, (R.K130000.7843.5F297) and Japan International Cooperation Agency (JICA) under grant (S.K130000.0543.4Y191). The authors also wish to acknowledge the National Hydraulic Research Institute of Malaysia (NAHRIM) for the facilities provided.

## References

Allen, L., D, W., Henning, D.L., Lee, 2007. Drilling riser fairing tests at prototype Reynolds numbers. In: International Conference on Offshore Mechanics and Arctic Engineering, 4269, pp. 793–802. https://doi.org/10.1115/OMAE2007-29219.

Bearman, P.W., 1984. Vortex shedding from oscillating bluff bodies. Ann. Rev. Fluid Mechanicsnnual Rev. Fluid Mech. 16 (1), 195–222. https://doi.org/10.1146/annurev.fl.16.010184.001211 no.

A.J. Brown, A. Universal, and R. King, "OTC 19161 Tests with a Flexible Quasi- Fairing to Reduce Riser Drag, Suppress VIV and Limit Drilling Down-Time," 2008.

Cicolin, M.M., Assi, G.R.S., 2017a. Experiments with flexible shrouds to reduce the vortex-induced vibration of a cylinder with low mass and damping. Appl. Ocean Res. 65, 290–301. https://doi.org/10.1016/j.apor.2017.04.003.

Cicolin, M.M., Assi, G.R.S., 2017b. Laboratory-scale investigation of the Ventilated-Trousers device acting as a suppressor of vortex-induced vibrations. Ocean Eng. 142 (May), 411–418. https://doi.org/10.1016/j.oceaneng.2017.07.024.

Cicolin, G.R., Freire, M.M., Assi, C.M., 2014. Suppression of the vortex-induced vibration of a circular cylinder with permeable meshes. In: Fluids Engineering Division Summer Meeting, 46223. https://doi.org/10.1115/FEDSM2014-22149 vol. V01BT12A011.

Gao, Y., Fu, S., Ren, T., Xiong, Y., Song, L., 2015. VIV response of a long flexible riser fitted with strakes in uniform and linearly sheared currents. Appl. Ocean Res. 52, 102–114. https://doi.org/10.1016/j.apor.2015.05.006.

Gonçalves, A.L.C., Rosetti, R.T., Franzini, G.F., Meneghini, G.R., Fujarra, J.R., 2013. Two-degree-of-freedom vortex-induced vibration of circular cylinders with very low aspect ratio and small mass ratio. J. Fluids Struct. 39, 237–257. https://doi.org/10.1016/j.jfluidstructs.2013.02.004.

Huera-Huarte, F.J., 2017. Suppression of vortex-induced vibration in low mass-damping circular cylinders using wire meshes. Mar. struct. 55, 200–213. https://doi.org/10.1016/j.marstruc.2017.05.008.

Jiménez-gonzález, J.I., Huera-huarte, F.J., 2018. Vortex-induced vibrations of a circular cylinder with a pair of control rods of varying size. J. Sound. Vib. 431, 163–176. https://doi.org/10.1016/j.jsv.2018.06.002.

Katopodes, Nikolaos D., 2018. Free-Surface Flow: Environmental Fluid Mechanics. Butterworth-Heinemann.

Khalak, A., Williamson, C.H.K., 1997. Fluid forces and dynamics of a hydroelastic structure with very low mass and damping. J. Fluids Struct. 11 (8), 973–982. https://doi.org/10.1006/jfls.1997.0110.

Khalak, A., Williamson, C.H.K., 1999. Motions, forces and mode transitions in vortex-induced vibrations at low mass-damping. J. Fluids Struct. 13 (7–8), 813–851. https://doi.org/10.1006/jfls.1999.0236.

Kim, D.K., Incecik, A., Choi, H.S., Wong, E.W.C., Yu, S.Y., Park, K.S., 2018. A simplified method to predict fatigue damage of offshore riser subjected to vortex-induced vibration by adopting current index concept. Ocean Eng. 157 (March), 401–411. https://doi.org/10.1016/j.oceaneng.2018.03.042.

King, H., Brown, R., Braaten, A., Russo, H., Baarholm, M., Lie, R., 2013. Suppressing full-scale riser VIV with the VT suppressor. In: International Conference on Offshore Mechanics and Arctic Engineering, 55416 vol.no. p. V007T08A085.

Kumar, N., Kumar Varma Kolahalam, V., Kantharaj, M., Manda, S., 2018. Suppression of vortex-induced vibrations using flexible shrouding—An experimental study. J. Fluids Struct. 81, 479–491. https://doi.org/10.1016/j.jfluidstructs.2018.04.018.

Liu, G., Li, H., Qiu, Z., Leng, D., Li, Z., Li, W., 2020. A mini review of recent progress on vortex-induced vibrations of marine risers. Ocean Eng. 195 (March 2019), 106704 https://doi.org/10.1016/j.oceaneng.2019.106704.

Park, S.J., Lee, C.W., 2002. Flow structure around a finite circular cylinder embedded in various atmospheric boundary layers. Fluid Dyn. Res. 30 (4), 197.

M.F. Praveen Duddu, "The world's worst offshore oil rig disasters," *7 July* 2021. https://www.offshore-technology.com/features/feature-the-worlds-deadliest-offshore-oil-rig-disasters-4149812/.

Qu, Y., Metrikine, A.v., 2020. A single van der pol wake oscillator model for coupled cross-flow and in-line vortex-induced vibrations. Ocean Eng. 196 (June 2019), 106732 https://doi.org/10.1016/j.oceaneng.2019.106732.

Quen, L.K., Abu, A., Kato, N., Muhamad, P., Tan, L.K., Kang, H.S., 2018. Performance of two- and three-start helical strakes in suppressing the vortex-induced vibration of a

low mass ratio flexible cylinder. Ocean Eng. 166, 253–261. https://doi.org/10.1016/j.oceaneng.2018.08.008.

E.R. Ranjith, A.S. Sunil, and L. Pauly, "Analysis of flow over a circular cylinder fitted with helical strakes," vol. 24, pp. 452–460, 2016, doi: 10.1016/j.protcy.2016.05.062.

Schlichting, H., 1968. Boundary-Layer Theory, 6th ed. McGraw Hill Book Company.

Senga, H., Kawasaki, S., Inoue, M., 2018. Study on the shape of buoyancy body for vortex induced vibration suppression. J. Japan Soc. Naval Architect. Ocean Eng. 27 (0), 99–105. https://doi.org/10.2534/jjasnaoe.27.99.

Silva-Ortega, M., Assi, G.R.S., 2017. Suppression of the vortex-induced vibration of a circular cylinder surrounded by eight rotating wake-control cylinders. J. Fluids Struct. 74, 401–412. https://doi.org/10.1016/j.jfluidstructs.2017.07.002.

J. Sumer, B., Fredsoe, "Hydrodynamics around Cyclindrical structures," vol. 26, 1997, doi: 10.1142/3316.

Jason Tranter, "RESONANCE the silent killer of rotating machinery," *April 18*, 2015. https://www.maintworld.com/Applications/RESONANCE-The-Silent-Killer-of-Rotating-Machinery.

Usta, O., Duranay, A., 2020. Uncertainty Analysis of Experiments of Vortex-Induced Vibrations for Circular Cylinders. J. Appl. Fluid Mech. 14 (2), 541–553. https://doi.org/10.47176/jafm.14.02.31778.

M.M. Zdravkovich and J.R. Volk~, "Effect of shroud geometry on the pressure distributed around a circular cylinder," 1972.

Zhou, T., Razali, S.F.M., Hao, Z., Cheng, L., 2011. On the study of vortex-induced vibration of a cylinder with helical strakes. J. Fluids Struct. 27 (7), 903–917. https://doi.org/10.1016/j.jfluidstructs.2011.04.014.

Zhu, H., Yao, J., 2015. Numerical evaluation of passive control of VIV by small control rods. Appl. Ocean Res. 51, 93–116. https://doi.org/10.1016/j.apor.2015.03.003.

Zhu, H., Liao, Z., Gao, Y., Zhao, Y., 2017. Numerical evaluation of the suppression effect of a free-to-rotate triangular fairing on the vortex-induced vibration of a circular cylinder. Appl. Math. Model. 52, 709–730. https://doi.org/10.1016/j.apm.2017.07.045.